Journal of Materials Chemistry A

PAPER

View Article Online
View Journal | View Issue

Cite this: J. Mater. Chem. A, 2014, 2, 15132

Surface-nanostructured cactus-like carbon microspheres for efficient photovoltaic devices†

Longbin Qiu,[a] Yi Jiang,[b] Xuemei Sun,[a] Xikui Liu*[b] and Huisheng Peng*[a]

Received 12th June 2014
Accepted 16th July 2014

DOI: 10.1039/c4ta02979h

www.rsc.org/MaterialsA

A constitutional dynamic chemistry process is developed to synthesize novel cactus-like nanostructured carbon microspheres with high specific surface areas and catalytic activities. Polyazomethine microspheres have been firstly synthesized from two representative monomers of 1,4-terephthalaldehyde and 3,5-diamino-1,2,4-triazole and then carbonized to produce the desired carbon nanomaterials. The morphologies of the surfaces on the carbon microspheres can be controlled with tunable roughness by introducing 2-aminopyridine. As an application demonstration, these nanostructured carbon microspheres are used as counter electrodes to fabricate efficient dye-sensitized solar cells with energy conversion efficiencies up to 7.5%.

Introduction

Carbon nanostructured materials including three-dimensional mesoporous carbon,[1] two-dimensional graphene,[2] one-dimensional carbon nanotubes[3] and zero-dimensional spheres[4] have been widely studied for high performance chemical and physical properties and promising applications in a wide variety of fields. For instance, these carbon nanomaterials are extensively used as electrodes to fabricate various high performance energy devices such as dye-sensitized solar cells,[5,6] electrochemical capacitors[7,8] and lithium ion batteries.[9,10] To this end, carbon spheres represent one of the most potential systems as they can be easily carbonized from polymer spheres through a low cost process at a large scale aiming at practical applications.[11,12] A lot of synthetic methods are used to synthesize building polymer spheres for carbonization to make carbon spheres.[13–15] However, it remains difficult to accurately control the structure of the carbon nanomaterials, *e.g.*, the roughness of the surface that may determine the efficiency on charge separation and transport. Constitutional dynamic chemistry (CDC) involves the formation of a series of molecular constituents through reversible covalent bonds, and it may offer a general and efficient approach to control the structure of polymers.[16,17] However, it is rare to use CDC to synthesize conducting polymer materials that may carbonize to produce carbon nanomaterials.

Polyazomethine, a Schiff base, is recently investigated as a functional conducting polymer with high thermal stability and mechanical property.[18–21] Due to its excellent optoelectronic properties, it has been widely studied for various photovoltaic devices.[22–28] This conducting polymer is generally synthesized by polycondensation that produces irregular precipitates.[29] Although the exchange reactions among Schiff base monomers are well recognized as an effective method in the preparation of polyazomethine for decades, it is rare to take advantage of such exchange reactions to tune the structure of polyazomethine or make polyazomethine materials with abundant nanostructures.

Herein, cactus-like polyazomethine microspheres with controlled nanostructures on the surface are synthesized from two monomers, *e.g.*, 1,4-terephthalaldehyde and 3,5-diamino-1,2,4-triazole, by the CDC method through a simple solution process. The following carbonization produces cactus-like carbon microspheres (hybridized with nitrogen) that inherit the nanostructured surface. These novel cactus-like carbon microspheres exhibit high surface areas and electrocatalytic activities. The nitrogen-doped carbon microspheres exhibited remarkable electrochemical catalytic activities, which is beneficial for the use as promising electrodes in various energy devices such as solar cells. As an application demonstration, they are used as high performance counter electrodes to fabricate dye-sensitized solar cells (DSCs) with energy conversion efficiencies up to 7.5%.

Experimental section

Morphosynthesis of polyazomethine and carbon microspheres

1,4-Terephthalaldehyde (TPA), 3,5-diamino-1,2,4-triazole (DAT), and 2-aminopyridine (AP) were ordered from Sigma-Aldrich and used as received. A mixture of isomers of dibenzyltoluene (DBT) was obtained from Yingkeli Co. Ltd. and used as received. In a typical synthesis, a DBT solution containing TPA and AP with

[a]State Key Laboratory of Molecular Engineering of Polymers, Department of Macromolecular Science and Laboratory of Advanced Materials, Fudan University, Shanghai 200438, China. E-mail: penghs@fudan.edu.cn

[b]College of Polymer Science and Engineering, Sichuan University, Chengdu 610065, China. E-mail: xkliu@scu.edu.cn

† Electronic supplementary information (ESI) available. See DOI: 10.1039/c4ta02979h

designed molar ratios was heated at 150 °C for 2 h to form a dynamic imine mixture. The solution was then heated to the reaction temperature of 220 °C, followed by addition of another DBT solution containing 3,5-diamino-1,2,4-triazole with an equal mole to TPA for *ca.* 10 s under stirring (solid content of 1 wt%). The polymerization was carried out for 6 h without stirring. The precipitate was collected and washed with ethanol at least three times and then dried in a vacuum at a temperature of 40 °C for 24 h. The carbonization of polyazomethine was made in argon for 120 min with a ramping rate of 10 °C min^{-1}.

Fabrication of DSCs

A carbon microsphere counter electrode was prepared by drop-casting a suspension of carbon microspheres dispersed in ethanol onto the F-doped tin oxide conducting glass substrate. The counter electrode was dried in a hot plate at 120 °C. The counter electrode was then heated at 500 °C in argon for 30 min for a better contact prior to use. For the platinum counter electrode, it was prepared by coating $H_2Pt_2Cl_6$ onto the conducting glass, followed by a thermal decomposition at 500 °C in air for 30 min.

The fabrication process is summarized below. The working electrode was prepared by a screen printing technology and composed of a layer of nanocrystalline TiO_2 (diameter of 20 nm) with a thickness of 14 μm and a light-scattering layer of TiO_2 (diameter of 200 nm) with a thickness of 2 μm. The working electrode was annealed at 500 °C for 30 min in air. It was then immersed in an aqueous solution of $TiCl_4$ (40 mM) at 60 °C for 20 min and washed with ethanol, followed by sintering at 500 °C for 30 min. After the temperature was cooled down to 120 °C, it was immersed into an N719 solution (0.3 mM) in dry acetonitrile and *tert*-butanol (volume ratio of 1/1) for 16 h. The working and counter electrodes with a Surlyn as the spacer were sealed by pressing them together at a pressure of 0.2 MPa and a temperature of 125 °C. The redox electrolyte (composed of 0.1 M lithium iodide, 0.05 M iodine, 0.6 M 1,2-dimethyl-3propylimidazolium iodide and 0.5 M 4-*tert* butyl-pyridine in dry acetonitrile) was introduced to the cell through the back hole of the counter electrode.[30]

Characterization

The morphologies were characterized by SEM (Hitachi FE-SEM S-4800 operating at 1 kV) and TEM (JEOL JEM-2100F operating at 200 kV). The chemical structures were characterized by Infrared (IR) spectroscopy (Shimadzu IRPrestige-21). X-ray photoelectron spectroscopy experiments were carried out on a RBD upgraded PHI-5000C ESCA system (Perkin Elmer) with Mg Kα radiation ($h\nu = 1253.6$ eV). Nitrogen sorption isotherms were performed on a Micromeritics ASAP 2020 analyzer at 77 K. Raman spectra ware recorded on inVia Raman microscopes (Renishaw). *J–V* curves were recorded using a Keithley 2400 Source Meter under illumination (100 mW cm^{-2}) of simulated AM1.5 solar light coming from a solar simulator (Oriel-Sol3A 94023A equipped with a 450 W Xe lamp and an AM1.5 filter). The light intensity was calibrated using a reference Si solar cell (Oriel-91150). The Tafel curves were performed on a CHI660a electrochemical workstation. Cyclic voltammetry measurements was performed in 1 mM I_2, 10 mM LiI and 0.1 M $LiClO_4$ acetonitrile solution at a scan rate of 100 mV s^{-1} through a three-electrode setup.

Results and discussion

The reactions in Schiff base involve a number of reversible steps that lead to the formation of dynamic imine bonds.[31] These imine bonds may be attacked by primary amines to produce aminals. According to this mechanism, polyazomethine microspheres are synthesized by the CDC method (Scheme 1). The clear reaction solution for the TPA and/or AP in DBT became turbid immediately after the addition of DAT due to the formation of polyazomethine precipitates.

The resulting polyazomethine precipitants were characterized by scanning electron microscopy (SEM) and transmission electron microscopy (TEM). Without the use of AP, polyazomethine precipitates display relatively smooth surfaces with irregular morphologies and sizes up to hundreds of micrometers (Fig. S1†). Interestingly, when AP was firstly mixed with TPA to form a dynamic imine mixture prior to the addition of DAT, the surface morphology was changed significantly, *i.e.*, cactus-

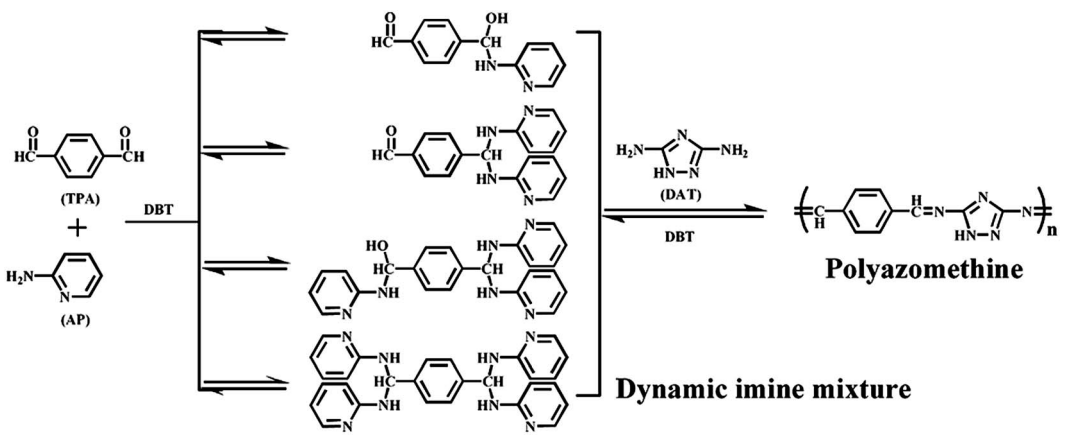

Scheme 1 Synthesis of polyazomethines through a constitutional dynamic chemistry reaction.

like microspheres were obtained. A series of polyazomethine materials had been synthesized by increasing the molar ratio between AP and TPA with the same TPA and DAT, and the samples are labelled as TPA-*x*AP-DAT with *x* as the AP/TPA molar ratio for the convenience of discussion. Compared with the case where no AP was used in Fig. S1,† a lot of thorns were vertically grown from the surface of the microspheres with the addition of AP (Fig. 1).

Note that when AP was added, dynamic imine mixtures were produced. After the diamine monomer DAT was added, polyazomethine was formed through an imine exchange polycondensation, while the AP was evaporated from the solution due to the high reaction temperature in the open reaction system. Therefore, the four polyazomethines shared the chemical structure (labelled as TPA-DAT), and the AP was varied mainly to tune the surface morphology of the resulting materials based on the reaction-induced crystallization mechanism.[32] After the mixture of TPA and DAT monomers at high temperatures, polycondensation started and the reaction solution became turbid immediately. When the TPA was reacted with AP to form dynamic imine mixtures, it would affect the polycondensation kinetics and reaction-induced crystallization. With the increasing AP molar ratio, more polyazomethine would crystallize on the surface of the spheres to form thorns. In other words, the surface roughness of the polyazomethine microsphere was controlled by varying the AP content.

The structures of polyazomethine microspheres were studied by Fourier transform infrared spectroscopy (FTIR) (Fig. 2), and the four samples shared similar spectra, so did the UV-vis spectra (Fig. S2†). The characteristic C=O stretch at 1690 cm^{-1} for the primary TPA was almost unavailable while a strong imine C=N stretch at 1605 cm^{-1} can be clearly observed, which verified the backbone structure for polyazomethine.

Aromatic polyazomethine shows a high char yield, which enables an efficient route to synthesize high performance carbon microspheres as the designed nanostructure on the polymer microspheres can be well maintained with high stability.[16] Fig. S3† shows the thermogravimetric analysis curves of polyazomethine synthesized from TPA and DAT. The weight loss of polyazomethine microspheres mainly occurred at a temperature range of 400–600 °C and a weight percentage of around 50% remained at 600 °C. The carbonized microspheres well inherited the size and cactus-like surface (Fig. 3), *e.g.*, diameters of 0.86, 1.47, 0.95 and 1.17 μm at the AP/TPA molar ratios of 1, 2, 3 and 4, respectively. No obvious dependence of the diameter on the AP/TPA molar ratio was observed. In contrast, the lengths of the nanostructured thorns on the surface were increased from 65, 92, 148 to 210 nm with the increasing AP/TPA ratio from 1, 2, 3 to 4, respectively (Fig. 4 and S4†). In addition, with the increasing AP/TPA molar ratio, the

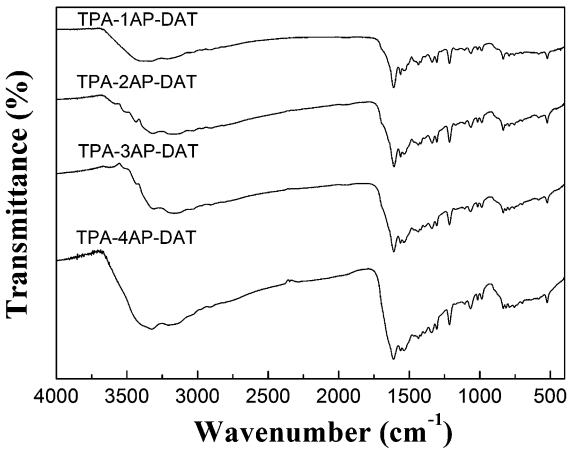

Fig. 2 FTIR spectra of polyazomethines synthesized from TPA-*x*AP-DAT ($x = 1, 2, 3, 4$) at 220 °C.

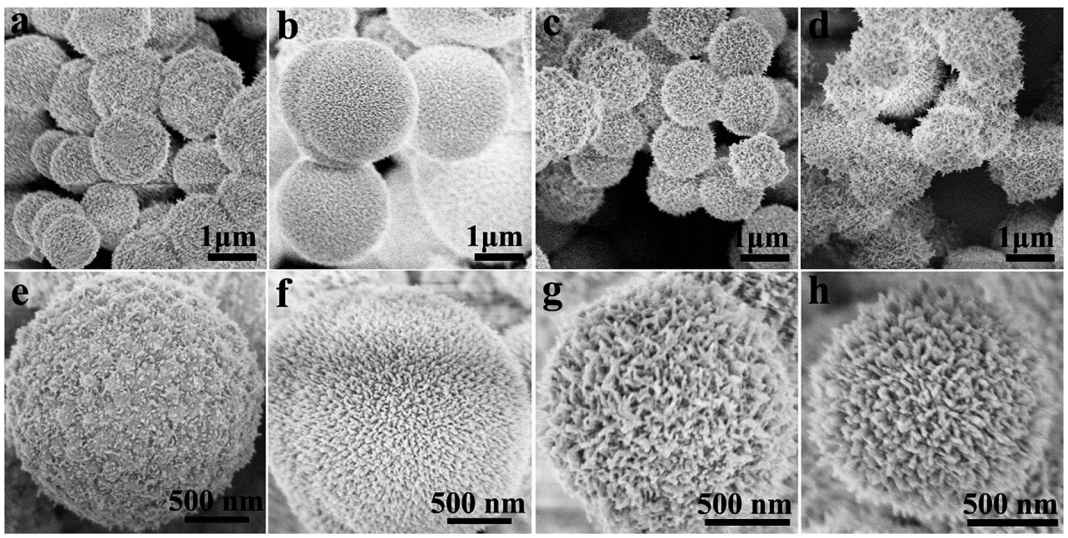

Fig. 1 TPA-DAT polyazomethine microspheres with controlled surface roughness through CDC controlled reaction. (a and e) TPA-1AP-DAT. (b and f) TPA-2AP-DAT. (c and g) TPA-3AP-DAT. (d and h) TPA-4AP-DAT.

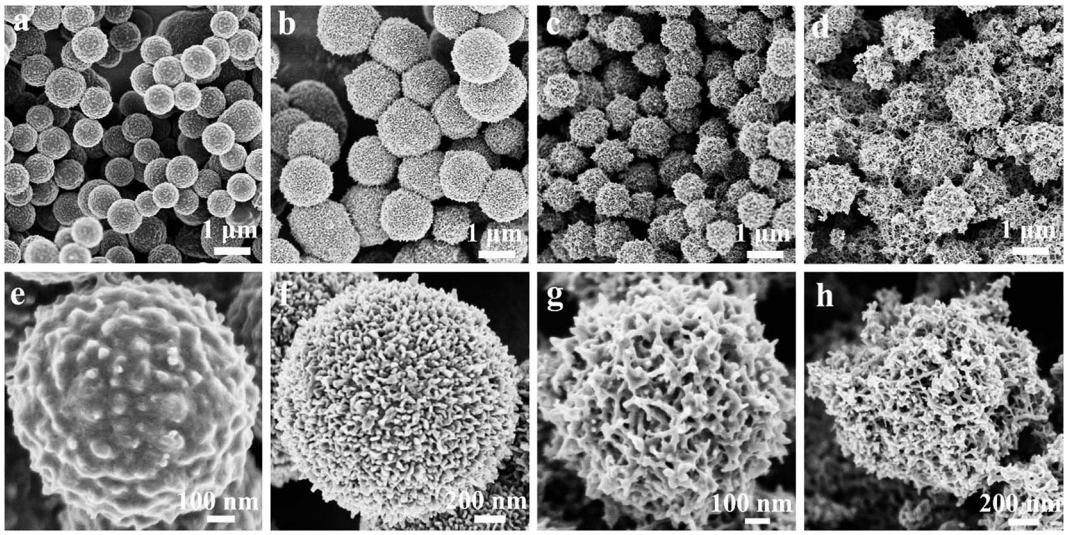

Fig. 3 SEM images of carbon microspheres after carbonization of TPA-DAT polyazomethines at low (a–d) and high (e–h) magnifications. (a and e) TPA-1AP-DAT. (b and f) TPA-2AP-DAT. (c and g) TPA-3AP-DAT. (d and h) TPA-4AP-DAT.

surface structures were changed from nanoparticles to nanofibers. In other words, the nanofibers had been gradually grown from the nanoparticles in a perpendicular direction relative to the spherical surface.

The Brunauer–Emmett–Teller surface areas of the nanostructured carbon microspheres have been further analyzed. The surface areas were measured as 219.5, 173.7, 293.9 and 248.6 $m^2\ g^{-1}$ at the AP/TPA molar ratios of 1, 2, 3 and 4, respectively. The high surface area may be attributed to the nanostructured surface of carbon microspheres as no mesopores were observed in sorption isotherms (Fig. S5†). Note that the specific surface areas of the carbon spheres did not increase with the increasing roughness (Fig. 4). This phenomenon may be explained by the different diameters of carbon microspheres in Fig. 3. For the resulting carbon microspheres at TPA-2AP-DAT, the diameter was the largest in the four carbon spheres, so the lowest specific surface area had been observed. A combined effect of the surface nanostructure and the diameter of carbon spheres enabled the highest specific surface area in the case of TPA-3AP-DAT. The surface of the carbon microsphere was also investigated by X-ray photoelectron spectroscopy. A close nitrogen content was obtained with the increasing AP/TPA molar ratio from 1 to 4 (Fig. S6†). Elemental analysis is further made to provide the content of the four materials (Table S1†). The incorporated nitrogen in the carbon microsphere had been previously shown to be useful in improving the electrocatalytic activity for various energy conversion and storage devices.[33]

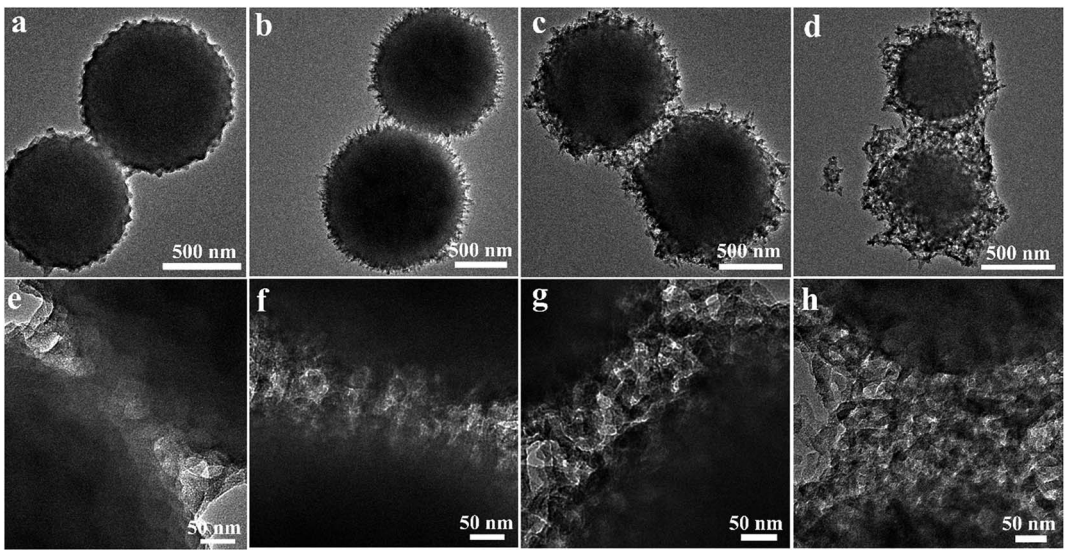

Fig. 4 TEM images of carbon microspheres after carbonization of TPA-DAT polyazomethines at 800 °C at low (a–d) and high (e–h) magnifications. (a and e) TPA-1AP-DAT. (b and f) TPA-2AP-DAT. (c and g) TPA-3AP-DAT. (d and h) TPA-4AP-DAT.

DSCs have been widely studied as a promising direction in photovoltaic devices due to low costs and high energy conversion efficiencies.[34] Recent interests are attracted to improve the performance by developing new materials for efficient electrodes, particularly, counter electrodes.[35] Platinum has been most explored for the counter electrode in DSCs. However, there is a limited source for platinum on earth, a high temperature or vacuum is required to prepare the platinum electrode with high cost, and platinum may be also dissolved in the used corrosive electrolyte. As a result, a wide variety of other materials such as carbon has been studied to replace platinum,[36] though the photovoltaic performance needs to be enhanced.

Here the carbon microspheres with high surface areas had been used as counter electrodes to fabricate efficient DSCs. Fig. 5a exhibits *J–V* curves of DSCs by using the carbon microspheres derived from TPA-*x*AP-DAT as counter electrodes. Here the nanostructured carbon spheres were coated onto the F-doped tin oxide and further annealed to enhance the contact. The DSCs fabricated from TPA-3AP-DAT typically showed a short-circuit current density (J_{SC}) of 14.99 mA cm^{-2}, open-circuit voltage (V_{oc}) of 0.73 V, and fill factor (FF) of 0.69. A maximal energy conversion efficiency (η) of 7.5% had been achieved, which is comparable to a platinum counter electrode (Fig. S7†). The DSCs fabricated from the other carbon spheres exhibited relatively lower short-circuit current densities and energy conversion efficiencies. To understand the performance of the nanostructured carbon spheres as counter electrodes, they were further investigated by measuring their catalytic activities on the redox reaction of I^-/I_3^- through the cyclic voltammetry (Fig. 5b). As expected, two pairs of oxidation and reduction peaks were clearly observed with the left and right pairs being ascribed to eqn (1) and (2), respectively.[37]

$$I_3^- + 2e^- \leftrightarrow 3I^- \quad (1)$$

$$3I_2 + 2e^- \leftrightarrow 2I_3^- \quad (2)$$

As the counter electrode of a DSC is mainly used to collect electrons and catalyze the reduction of I_3^- to I^-, the left pair becomes critically important for these materials. The peak current density and peak-to-peak separation voltage are generally used to evaluate catalytic activities of counter electrodes. Carbon spheres derived from TPA-3AP-DAT exhibited higher current densities than the other carbon spheres due to the highest specific surface area for both electron collection and transport.

With the increasing carbonization temperature, the graphitization degrees were increased and could also affect the photovoltaic performance in DSCs. To take TPA-4AP-DAT as an example, with increasing carbonization temperature from 700 to 1000 °C, the intensity ratio between G and D bands in Raman spectra were gradually increased from 0.94 to 1.15 with decreasing defects (Fig. S8†). The defects of the disordered graphitic structure acted as catalytically active sites for efficient DSCs.[38] Fig. 6a shows typical *J–V* curves of DSCs fabricated with

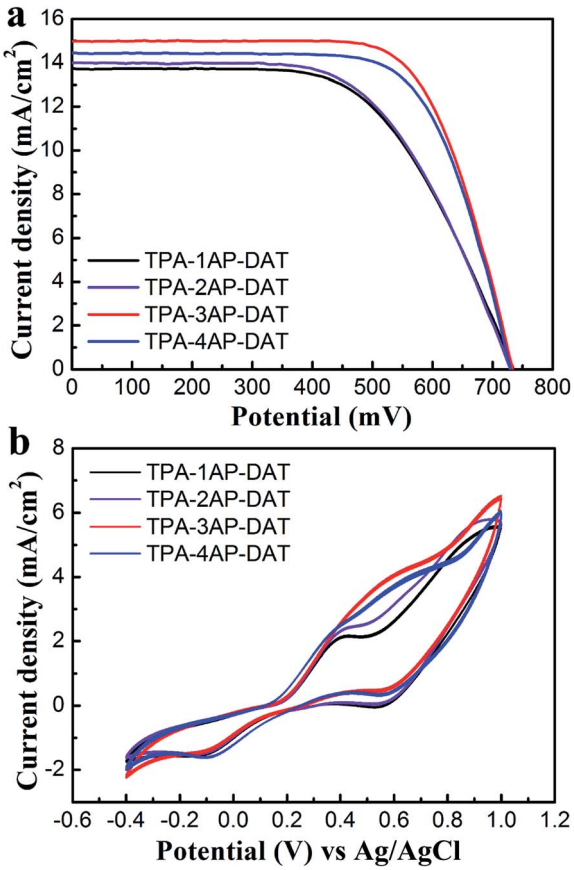

Fig. 5 *J–V* (a) and CV (b) curves of counter electrodes derived from different surface-nanostructured polyazomethine microspheres after carbonization at 800 °C.

carbon spheres derived from TPA-4AP-DAT and carbonized at the range of 700 to 1000 °C. For carbon spheres carbonized at a lower temperature of 700 °C, a low FF and a low η were produced due to poor conductivity of carbon spheres. With increasing carbonized temperatures, the FF was gradually increased. In contrast, the catalytic properties were decreased with the increasing graphitization degree. As a balance, a maximal J_{SC} was observed at a carbonization temperature of 800 °C. Fig. 6b exhibits the Tafel curves of electrodes fabricated with carbon spheres carbonized at different temperatures. The slopes for the anodic or cathodic branches were found in the order of 800 °C > 700 °C > 900 °C > 1000 °C. A larger slope indicated a higher exchange current density in the electrode.[39] In addition, the Tafel polarization curves indicated the order of limiting current densities,[40] *i.e.*, 700 or 800 °C > 900 °C > 1000 °C, which is consistent with the order of photovoltaic performance in the DSCs. Therefore, a carbonization at 800 °C provided carbon spheres with the highest catalytic activity and charge transport.

In summary, a new family of cactus-like nanostructured carbon microspheres have been synthesized from polyazomethine microspheres based on a constitutional dynamic chemistry reaction. These nanostructured carbon spheres show a controlled surface roughness and high specific surface areas

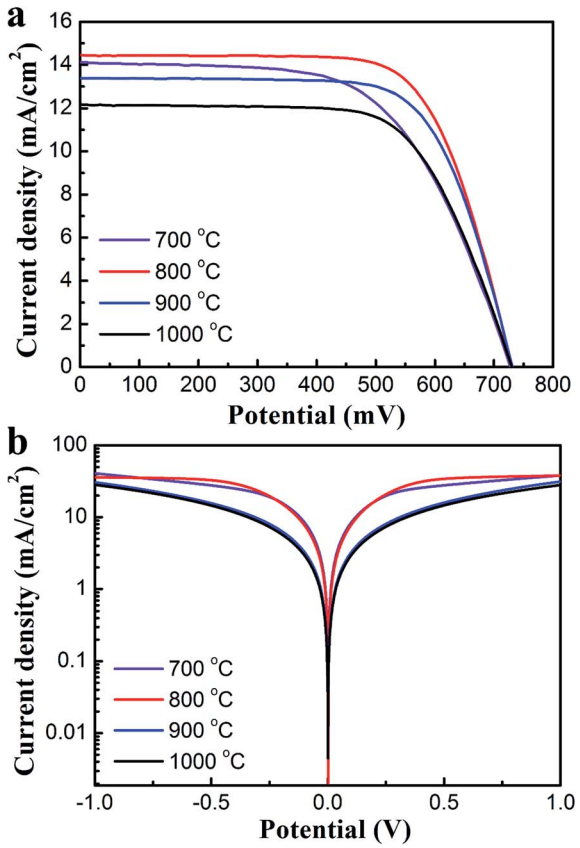

Fig. 6 *J–V* (a) and Tafel (b) curves of counter electrodes derived from TPA-4AP-DAT carbonized at increasing temperatures from 700 to 1000 °C in an argon atmosphere.

that enable a remarkable electrocatalytic activity. They have been further developed as promising counter electrodes to fabricate efficient DSCs.

Acknowledgements

This work was supported by MOST (2011CB932503), NSFC (21225417, 21174089), STCSM (12nm0503200), the Fok Ying Tong Education Foundation, the Program for Special Appointments of Professors at Shanghai Institutions of Higher Learning, and the Program for Outstanding Young Scholars from the Organization Department of the CPC Central Committee, and the State Key Laboratory of Molecular Engineering of Polymers (Fudan University) (no. K2013-23).

References

1 R. Ryoo, S. H. Joo, M. Kruk and M. Jaroniec, *Adv. Mater.*, 2001, **13**, 677–681.
2 X. Li, W. Cai, J. An, S. Kim, J. Nah, D. Yang, R. Piner, A. Velamakanni, I. Jung, E. Tutuc, S. K. Banerjee, L. Colombo and R. S. Ruoff, *Science*, 2009, **324**, 1312–1314.
3 M. F. De Volder, S. H. Tawfick, R. H. Baughman and A. J. Hart, *Science*, 2013, **339**, 535–539.
4 X. Sun and Y. Li, *Angew. Chem., Int. Ed.*, 2004, **43**, 597–601.
5 Z. Yang, T. Chen, R. He, G. Guan, H. Li, L. Qiu and H. Peng, *Adv. Mater.*, 2011, **23**, 5436–5439.
6 X. Wang, L. Zhi and K. Mullen, *Nano Lett.*, 2008, **8**, 323–327.
7 J. Ren, W. Bai, G. Guan, Y. Zhang and H. Peng, *Adv. Mater.*, 2013, **25**, 5965–5970.
8 X. Yang, C. Cheng, Y. Wang, L. Qiu and D. Li, *Science*, 2013, **341**, 534–537.
9 A. C. Dillon, *Chem. Rev.*, 2010, **110**, 6856–6872.
10 H. S. Zhou, S. M. Zhu, M. Hibino, I. Honma and M. Ichihara, *Adv. Mater.*, 2003, **15**, 2107–2111.
11 Y. Z. Jin, C. Gao, W. K. Hsu, Y. Zhu, A. Huczko, M. Bystrzejewski, M. Roe, C. Y. Lee, S. Acquah, H. Kroto and D. R. M. Walton, *Carbon*, 2005, **43**, 1944–1953.
12 J. Gong, J. Liu, Z. Jiang, X. Chen, X. Wen, E. Mijowska and T. Tang, *Appl. Catal., B*, 2014, **152–153**, 289–299.
13 H. J. Lee, S. Choi and M. Oh, *Chem. Commun.*, 2014, **50**, 4492–4495.
14 M. Ju, C. Zeng, C. Wang and L. Zhang, *Ind. Eng. Chem. Res.*, 2014, **53**, 3084–3090.
15 J. Han, G. Xu, B. Ding, J. Pan, H. Dou and D. R. MacFarlane, *J. Mater. Chem. A*, 2014, **2**, 5352.
16 Y. Yan, L. Chen, H. Dai, Z. Chen, X. Li and X. Liu, *Polymer*, 2012, **53**, 1611–1616.
17 L. Chen, Z. Chen, X. Li, W. Huang, X. Li and X. Liu, *Polymer*, 2013, **54**, 1739–1745.
18 J. Cai, P. Zhao, H. Niu, Y. Lian, C. Wang, X. Bai and W. Wang, *Polym. Chem.*, 2013, **4**, 1183–1192.
19 B. Jarząbek, B. Kaczmarczyk, J. Jurusik and J. Weszka, *J. Non-Cryst. Solids*, 2013, **379**, 27–34.
20 A. Iwan and D. Sek, *Prog. Polym. Sci.*, 2008, **33**, 289–345.
21 A. Iwan and D. Sek, *Prog. Polym.Sci.*, 2011, **36**, 1277–1325.
22 M. Palewicz, A. Iwan, M. Sibinski, A. Sikora and B. Mazurek, *Energy Procedia*, 2011, **3**, 84–91.
23 A. Iwan, M. Palewicz, A. Chuchmała, L. Gorecki, A. Sikora, B. Mazurek and G. Pasciak, *Synthetic Met.*, 2012, **162**, 143–153.
24 A. Iwan, J. R. Guimarães, M. C. dos Santos, E. Schab-Balcerzak, M. Krompiec, M. Palewicz and A. Sikora, *High Perform. Polym.*, 2012, **24**, 319–330.
25 A. Iwan, M. Palewicz, A. Chuchmala, A. Sikora, L. Gorecki and D. Sek, *High Perform. Polym.*, 2013, **25**, 832–842.
26 A. Iwan, E. Schab-Balcerzak, K. P. Korona, S. Grankowska and M. Kamińska, *Synth. Met.*, 2013, **185–186**, 17–24.
27 J. C. Hindson, B. Ulgut, R. H. Friend, N. C. Greenham, B. Norder, A. Kotlewski and T. J. Dingemans, *J. Mater. Chem.*, 2010, **20**, 937–944.
28 G. D. Sharma, S. G. Sandogaker and M. S. Roy, *Thin Solid Films*, 1996, **278**, 129–134.
29 L. Song, C. Tu, Y. Shi, F. Qiu, L. He, Y. Jiang, Q. Zhu, B. Zhu, D. Yan and X. Zhu, *Macromol. Rapid Commun.*, 2010, **31**, 443–448.
30 L. Qiu, Q. Wu, Z. Yang, X. Sun, Y. Zhang and H. Peng, *Small*, 2014, DOI: 10.1002/smll.201400703.
31 R. W. Layer, *Chem. Rev.*, 1963, **63**, 489–510.
32 K. Wakabayashi, T. Uchida, S. Yamazaki and K. Kimura, *Macromolecules*, 2008, **41**, 4607–4614.

33 S. Hou, X. Cai, H. Wu, X. Yu, M. Peng, K. Yan and D. Zou, *Energy Environ. Sci.*, 2013, **6**, 3356.
34 B. E. Hardin, H. J. Snaith and M. D. McGehee, *Nat. Photonics*, 2012, **6**, 162–169.
35 S. Thomas, T. G. Deepak, G. S. Anjusree, T. A. Arun, S. V. Nair and A. S. Nair, *J. Mater. Chem. A*, 2014, **2**, 4474–4490.
36 W. Kwon, J.-M. Kim and S.-W. Rhee, *J. Mater. Chem. A*, 2013, **1**, 3202–3215.
37 F. Gong, H. Wang, X. Xu, G. Zhou and Z. S. Wang, *J. Am. Chem. Soc.*, 2012, **134**, 10953–10958.
38 J.-M. Kim and S.-W. Rhee, *Electrochim. Acta*, 2012, **83**, 264–270.
39 M. K. Wang, A. M. Anghel, B. Marsan, N. L. C. Ha, N. Pootrakulchote, S. M. Zakeeruddin and M. Grätzel, *J. Am. Chem. Soc.*, 2009, **131**, 15976–15977.
40 A. Hauch and A. Georg, *Electrochim. Acta*, 2001, **46**, 3457–3466.